Planing Boats in Waves

Authors:
Rodrigo Azcueta, MTG Marinetechnik GmbH, Germany
Mario Caponnetto, Rolla Research, Switzerland
Heinrich Söding, TU Hamburg Harburg, Germany

1 ABSTRACT

Three methods are described to simulate motions of planing boats in waves. One is based on Wagner's theory of hydrodynamic impacts, the others use the Ranse solver Comet, applying different concepts to adapt the computational grid to the boat motions. Comparisons with published experiments are used for validation and to demonstrate the difficulties of both experiments and simulations in evaluating the highly nonlinear responses in case of very high speed (Froude number ≈ 4).

2 INTRODUCTION

The design of a planing boat requires a trade-off between calm water resistance and seakeeping qualities. A fast hard-chine vessel with a flat bottom has lower resistance than one having a deadrise. In waves, however, a flat hull is one of the worst shapes to imagine, because large impact pressures are generated when waves hit the bottom. The best deadrise angle depends on expected waves and whether speed or comfort are more important, and it should be larger at the bow where the relative vertical motion between boat and water surface is larger than at the stern. Hydrodynamic calculations are used both for powering and seakeeping predictions. Here three different methods for simulating the boat's motions in waves are described and compared: A method by Söding based on an extension of Wagner's (1932) theory, and two different ways (one by Caponnetto, the other by Azcueta) of applying the RANSE solver Comet to this problem.

The assumption that boat motions depend linearly on wave amplitude is not valid for the very high speed case investigated here, even in waves of very moderate steepness. Often the boat jumps completely out of the water, flying

over the next wave trough and perhaps also over one, two or more successive wave crests. This leads to subharmonic motions, i.e. the motion period of the boat is an integer multiple of the wave encounter period. In higher waves the motions become chaotic.

3 THE WAGNER-TYPE METHOD

3.1 Basic equations

The vertical hydrodynamic force per length f on a boat section is determined by the "momentum equation" introduced to this problem by *v.Karman (1929)* and *Wagner (1932)*:

$$f = -k\frac{d}{dt}\left(\rho\frac{\pi}{4}c^2 V\right), \tag{1}$$

where $\rho\frac{\pi}{4}c^2$ approximates the added mass per length (for c see Fig. 1), V is downward velocity of the section relative to the water, and k is a correction factor. The rise of the waver level $T - T_0$ (Fig. 2) during immersion is approximated as $0.6A/c$ where A is the immersed section area. This implicit equation for T is solved by the iteration

$$T_{j+1} = T_j + \frac{c_j(T_0 - T_j) + 0.6A_j}{c_j - (T_0 - T_j)/\tan\alpha - 0.6c_j}\ . \tag{2}$$

For α (see Fig. 1), which influences the iteration but not the final result, the approximation

$$\bar{\alpha} = \arctan(2A/c^2) \tag{3}$$

is used. $\bar{\alpha}$ is also applied to reduce f for deep sections:

$$k = 0.75(\pi/2 - \bar{\alpha}). \tag{4}$$

The results of formulae (1–4) are compared to experimental results and detailed flow computations in Figs. 2 and 3.

3.2 Sections with knuckles; emerging sections

When a section having a knuckle (Fig. 15) is immersed beyond the knuckle, the flow separates from the section contour. To account for this approximately, above the knuckle the section halfbreadth is modified according to the formula

$$\frac{dc}{dz} = 0.64\left(1 - \frac{\bar{\alpha}_k}{\pi/2}\right), \tag{5}$$

where $\bar{\alpha}_k$ follows from (3) for immersion up to the knuckle.

For emergence of sections (V directed upward) further modifications are made; however, these occured seldom in the cases investigated here due to the aft trim in connection with the high forward speed.

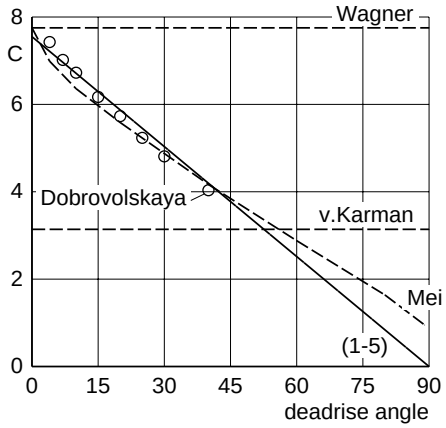

Fig. 2 . Vertical force on wedges depending on deadrise angle according to formulae of *v. Karman (1929)*, *Wagner(1932)*, and formulae (1-5), as well as computations of *Dobrovolskaya (1969)* and *Mei et al. (1999)*. $C = f \tan^2 \alpha / \rho V^3 t$. Without hydrostatic components.

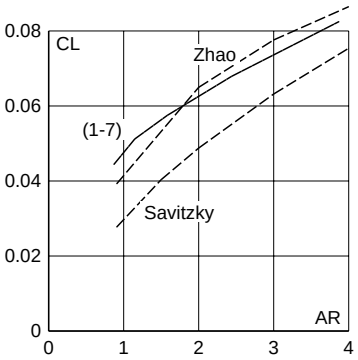

Fig. 4. Planing surface having 20° deadrise and 20° trim angle. CL =lift/(stagnation pressure · breadth^2) depending on AR =(average distance between transom and spray root)/breadth. Experiments by *Savitzky (1964)*, computations by *Zhao et al. (1997)*, and results of (1-7).

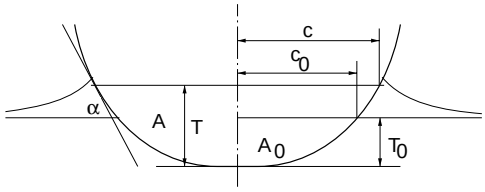

Fig. 1. Cross-section definitions

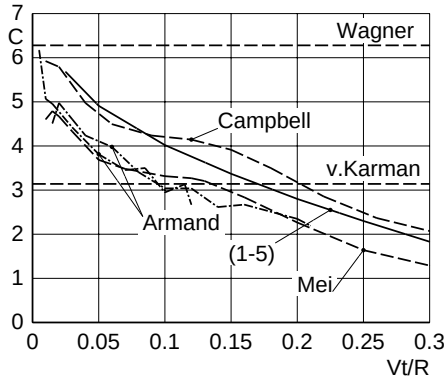

Fig. 3. Vertical force on a circular cylinder (radius R) depending on time t since water contact, according to formulae by *v. Karman (1929)*, *Wagner (1932)*, and according to (1-5), as well as computations by *Mei et al. (1999)* and experiments of *Campbell and Weynberg (1980)* and *Armand and Cointe (1987)*. $C = fl/\rho V^2 R$ with l =body length = 0.1m. Without hydrostatic components.

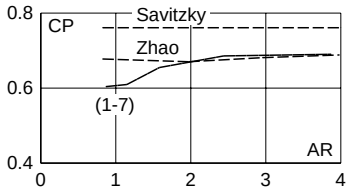

Fig. 5. Planing surface like in Fig. 5. CP = (distance between center of lift and transom)/ (average distance between transom and spray root).

3.3 Variable section shape and bodies with forward speed

For slender bodies with forward speed u in direction x, the time derivative d/dt in (1) has to be substituted by the substantial derivative

$$D/Dt = \partial/\partial t - u\partial/\partial x. \tag{6}$$

Also for V the substantial derivative of the bottom depth relative to the water surface has to be used. For lengthwise variable cross-sections an average

V over section breadth is defined as

$$V = \frac{1}{c}\frac{DA}{Dt} - \frac{D}{Dt}(T - T_0) = 0.4\frac{1}{c}\frac{DA}{Dt} + 0.6\frac{A}{c^2}\frac{Dc}{Dt}. \quad (7)$$

Figs. 5 and 6 compare results of these formulae with experimental and computed results for stationary planing.

3.4 Further details

From f (vertical force per length including buoyancy) the vertical pressure force and the pitch moment are integrated. Also the longitudinal pressure force per length f_x (excluding friction) can be approximated as $f_x = f/c \cdot dA/dx$. These 3 force quantities allow to integrate the surge, heave and pitch motion.

To allow large time steps an implicit time integration scheme is applied. From the results of the previous time and iteration steps the time-dependent added mass matrix is determined as explained by *Söding (2001)*. This avoids the necessity of force and moment fairing explained in 6.3. To start the simulation the boat is dropped from slightly above the water surface; this allows to set the added mass matrix initially to zero.

The hull shape is approximated by 100 to 200 cross sections each described by, typically, 150 halfbreadths between bottom and deck. This gives mesh-independent results and computing times on a PC which are, roughly, equal to or less than the simulated time span.

4 THE RANSE METHODS

The two other authors both used the Navier-Stokes solver Comet. It applies a finite-volume method, allowing unstructured and block-structured meshes with non-matching, sliding block interfaces. The mesh can move with time. The momentum equations take account of the additional terms caused by rotations and accelerations, and an additional "volume conservation equation" takes account of mesh deformations. This avoids any interpolation of variables from the old cell centres to the new ones. The free surface is accounted for by a volume-of-fluid method, which is well suited to deal with spray, breaking and overturning waves, detachment and reattachment of the flow along the chine, and – to some extent – with ventilation. The solution domain covers both the water and air region. Turbulence (here of minor importance) is approximated using a k-ϵ model.

5 METHOD BY CAPONNETTO

5.1 Body motion

At each time step updated values for trim and sinkage are supplied to a program to build the new mesh. The cell vertices on the external boundary remain fixed, while those on the hull move rigidly with the hull. All other vertices move by an appropriate fraction of the hull movements, keeping the

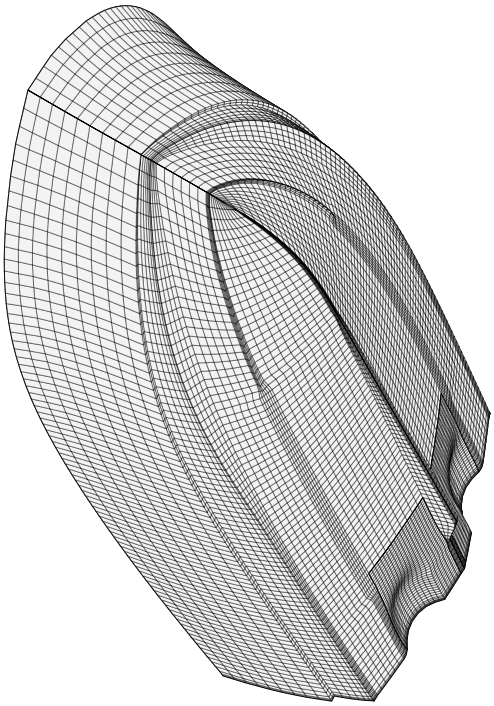

Fig. 6 (left). Computational mesh on the body surface of a planing boat with spray rails and propeller tunnels

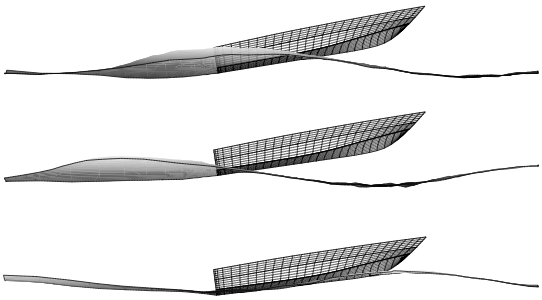

Fig. 7. Planing boat at different phases of wave encounter

same grid topology. Figs. 6 and 7 show an example of the body grid and of a planing boat in 3 different phases of wave contounter, respectively.

5.2 Boundary and initial conditions; time step

Momentum and velocity are expressed in the inertial system. At the inlet air, water or a mixture of both are blown in depending on the position of the cell above, below or at the actual surface height. Within the water pressure and velocity are enforced at the inlet corresponding to linear inviscid wave theory with a simple non-linear adaptation, whereas the air speed and pressure are kept constant at the inlet. Initially the free surface is flat, the flow has uniform velocity $(-v, 0, 0)$, and the pressure is static. The wave amplitude is then increased linearly from zero to H_w in about one encounter period. The integration over time is second-order implicit using results of 3 successive time instants; the time step is kept constant $= 0.15l/v$.

5.3 Forces and moments calculation

At the end of each time step the pressure over the hull is known, giving the vertical force and the pitch moment. Physically, due to added-mass effects the force and moment depend on the acceleration which is still not known. To avoid oscillations or instability, the computed force and moment are smoothed over time using, for instance, the last 10 time instants. The smoothed force and moment give the accelerations and thus the boat position at the next time step.

6 METHOD BY AZCUETA

6.1 Body motion module

Here the mesh is rigid and fixed to the boat. Momentum and velocity components refer to the boat-fixed reference system. A "body-motion module" is

linked and run simultaneously with the flow solver to update all flow variables, boundary conditions and parameters of the numerical method.

To integrate in time the equations of motion a first-order explicit discretisation method has shown to work well and is used preferably. To obtain the rotation angles, the new orientation of the body is found by integrating the unit vectors of the body-fixed coordinate system.

6.2 Numerical mesh and simulation set-up

For the planing boat model of Fig. 10 and Table 1, a single grid consisting of 230 000 control volumes for one of the two symmetric fluid flow regions was generated using the ICEM-CFD Hexa mesh generator. The pitch radius of gyration (not known from the experiments) was estimated as $0.2\,L_{oa}$.

The computational domain is shown in Fig. 8. Fig. 9 shows a part of the mesh. All outer planes except the back plane were specified as an inlet of constant known velocity (boat speed in opposite direction plus orbital velocity of the incoming waves) and known void fraction distribution defining the water and air regions. The aft flow-boundary was specified as a zero-gradient boundary of known (hydrostatic) pressure distribution.

The challenge of these simulations is the high F_n, which causes difficulties in generating the incident waves since the mean flow velocity due to the boat forward speed is 2 to 3 orders of magnitude larger than the wave orbital velocity. Special care is to be taken in selecting appropriate aspect ratios of CVs to avoid unphysical wave irregularities. Due to numerical diffusion the amplitude of the wave hitting the boat is smaller, although the VOF method used here produces surprisingly good results on relatively coarse meshes.

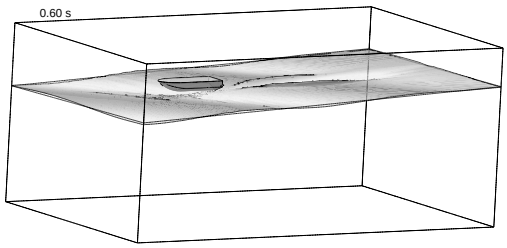

Fig. 8. Power boat model jumping in oblique waves at a speed of 9m/s.

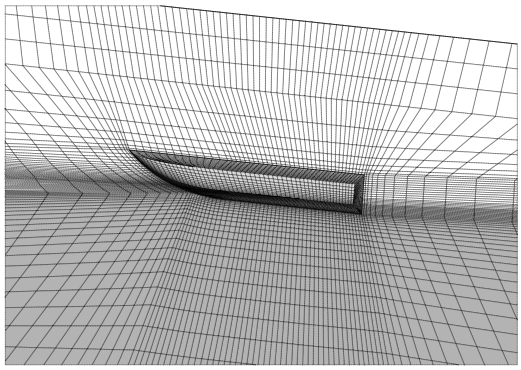

Fig. 9. Numerical mesh around hull viewed from the side.

The computational grid moves together with the boat, causing large motions of the water surface relative to the grid along the outer flow boundaries. Therefore the boundary conditions – the mean flow velocity, the orbital velocity, the void fraction distribution defining the wave elevations, the turbulence parameters and so on – have to be very carefully imposed at each time instant relative to the undisturbed waterplane. The VOF method and the implemented boundary conditions proved to be very robust: The free surface may,

e.g., intersect the top face of the outer boundary in case of large pitch or roll angle. Even capsizing of the boat may be handled by this method.

7 VALIDATION

For validating the 3 calculation methods we use experiments by *Katayama et al. (2000)*. The shape of their small model is described by Table 1 and Fig. 10. The model was towed with constant speed U at the center of gravity G; thus at G the surge motion was suppressed. The same was enforced in the simulations. The heave motion refers to G. In the experiments the model, floating initially in equilibrium condition, was accelerated within a very short time to the test speed. This differs from the starting procedure of the simulations and may have influenced the final, periodical motions in several of the cases investigated.

Table 1. Model data

length L_{OA}	0.625m	breadth B	0.250m
length L_{pp}	0.600m		
depth D	0.106m	draft d	0.059m
deadrise β	22°	mass m	4.28kg
KG	0.111m	LCG–trans.	0.285m

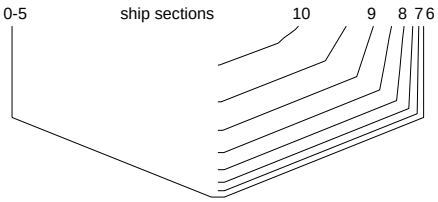

Fig. 10. Body plan of model

Fig. 11 shows nondimensional heave (maximum – minimum heave $Z(t)$ over wave height $H_w = 2 \cdot$ wave amplitude) plotted as a function of wave height made non-dimensional by dividing it by the draft at rest $d = .059$m. The boat sails in a regular wave of length $\lambda = 1.556$m at $F_n = 1.21$ which is a typical Froude number for planing boats. For the same case Fig. 12 gives nondimensional pitch = maximum – minimum pitch angle T_h divided by the (linear) wave slope double amplitude KH_w where K is wave number. The results apply to the stationary oscillation (limit cycle) of wave encounter period after the transients have died-out.

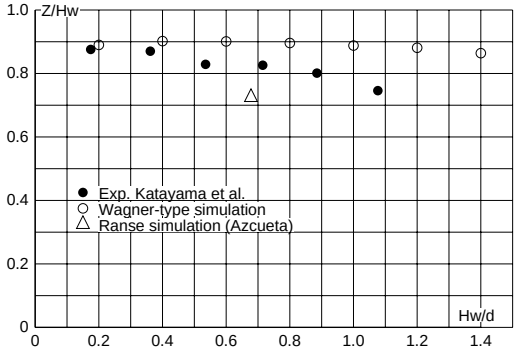

Fig. 11. Nondimensional heave over wave height; $\lambda/L_{OA} = 2.49, F_n = 1.21$.

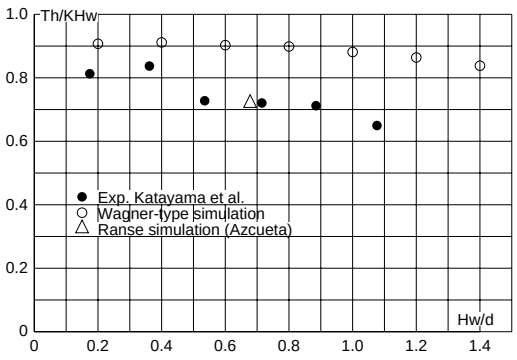

Fig. 12. Nondimensional pitch over wave height; $\lambda/L_{OA} = 2.49, F_n = 1.21$.

Corresponding results for the same wave length 1.556m but much higher $F_n = 3.63$ (model speed 9m/s) are shown in Figs. 13 and 14. Here the ship

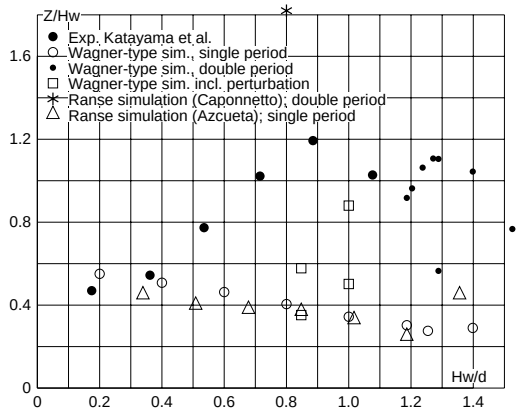

Fig. 13. Nondimensional heave over wave height; $\lambda/L_{OA} = 2.49, F_n = 3.63$.

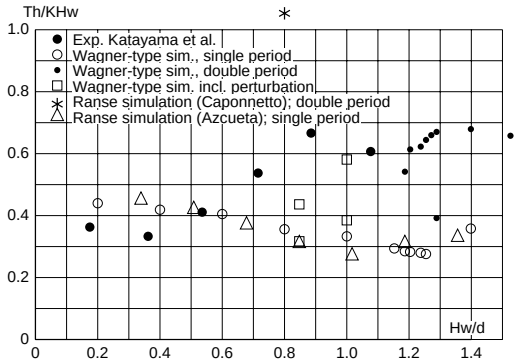

Fig. 14. Nondimensional pitch over wave height; $\lambda/L_{OA} = 2.49, F_n = 3.63$.

motions converge to a stationary oscillation of wave encounter frequency only for very low wave height. For somewhat larger wave height the motion repeats after twice the encounter period. According to the experiments the transition from single- to double-period motions seems to occur below $H_w/d = 1$. Also the Ranse simulation showed a double-period response for $H_w/d = 0.8$. In the Wagner-type simulations, however, single-period motions were found until about $H_w/d = 1.4$ but not beyond. Between $H_w/d = 1.2$ and 1.4 both single-period and double-period responses were found as limit cycles, depending on the initial drop conditions of the model. According to the latter simulations there is no smooth increase of the nondimensional motion transfer functions with wave height; instead, if two-period motions occur as the limit cycle, they have much larger amplitudes than the single-period responses. Occasionally also two different two-period limit cycles are found for the same wave and speed conditions but different initial conditions. Further, the distinction between one-period and two-period limit cycles is not always clear: sometimes even and odd cycles of wave encounter period differ only slightly from each other. The transition from an initial near-periodic response to the limit cycle may also appear after long times which may be too long for the experiments or Ranse simulations to discover it (Fig. 15).

For the experiments Katayama et al. reported irregular motions for $H_w/d > 0.7$. That could be understood as chaotic motions. In the Wagner-type simulations, however, two-period responses were found up to about $H_w/d = 1.35$, and chaotic motions appeared only for $H_w/d > 1.63$. Because in some experiments the wave tracks shown by the authors are far from sinusoidal, Wagner-type simulations were performed also in slightly perturbated waves (Fig. 16). This small irregularity, which appears much smaller than that shown in the experiments, produced, e.g. at $H_w/d = 1$ (Figs. 13, 14), dramatic changes in the responses, and it lowered the range were double-period responses were found. Thus the irregular measured motions may have been influenced by irregularities of the very flat waves.

All the above referred to waves of a single length $\lambda = 2.49 L_{OA}$. Figs. 17 and

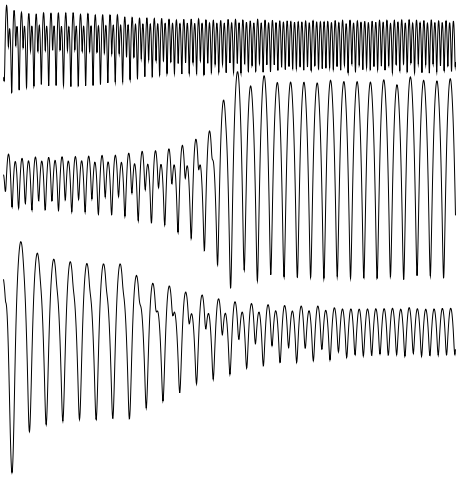

Fig. 15 (left). Simulated heave motions (Wagner-type method) in regular waves of 1.556m length for wave heights of 7.1cm (bottom), 7.55cm (middle) and 8.25cm (top). Different time scales (abszissa).

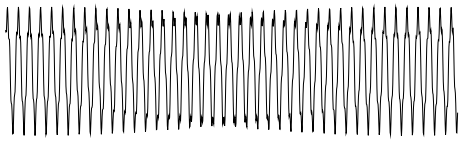

Fig. 16. Wave track with perturbation

18, on the other hand, show measured and simulated non-dimensional heave and pitch for variable (greater) wave length for a single wave height of 2cm. The large measured responses near $\lambda/L_{OA} = 5.5$) occur for an encounter period $T_e = 0.30$s which is not far from the natural pitch period measured for the same $F_n = 3.63$. In the Wagner-type simulations no sharp peak response was found, neither with regular nor with the disturbed waves, whereas both Ranse simulations gave results between the experiments and the Wagner-type simulations. For 4cm wave height the experiments showed a peak at a shorter wavelengh $\lambda/L_{OA} = 3$. Also that peak was not found in the simulations (Figs. 19, 20); however, the Ranse simulations by the Caponnetto method correspond better to the experiments than the Wagner-type simulations. (Actually the Ranse simulation for $\lambda/L_{OA} = 3.6$ was performed for 3 instead of 4 cm wave height.) In all the simulations of Figs. 17–20 the responses were periodic with the wave encounter period.

Fig. 21 shows average trim angle and standard deviation of pitch angle in natural long-crested head seaways containing wavelengths between about 0.95m and 2.3m, with maximum energy at about 1.6m wavelength. Here both the average trim and the standard deviation of pitch change continuously with significant wave height. Unfortunately no experimental data or RANSE simulations in irregular waves are available for comparison; the latter require prohibitively long CPU time.

8 CONCLUSIONS

1. Because the motions of planing boats in waves are highly nonlinear even for small wave steepness, nonlinear simulations are the appropriate tool for predicting the motions of planing boats in waves.

2. For the very high Froude numbers investigated here, even in quite flat waves the boat experiences subharmonic motions often accompanied with jumping over one or more wave crests.

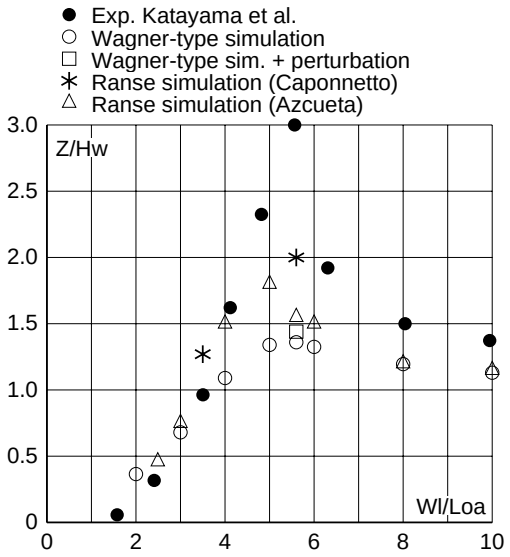

Fig. 17. Non-dimensional heave over nondimensional wave length for $H_w =$ 2cm and $U = 9$m/s

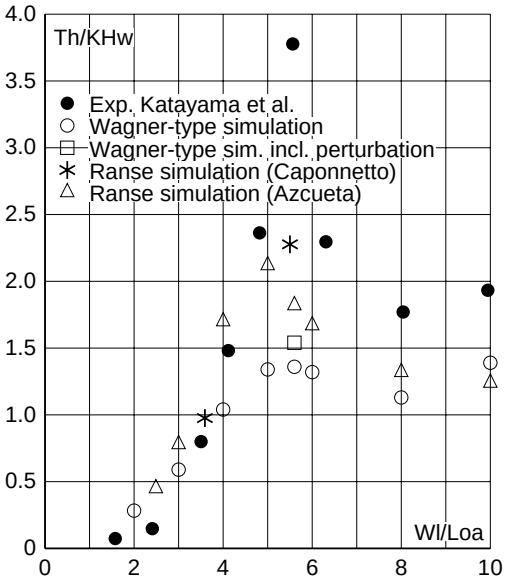

Fig. 18. Non-dimensional pitch over nondimensional wave length for $H_w =$ 2cm and $U = 9$m/s

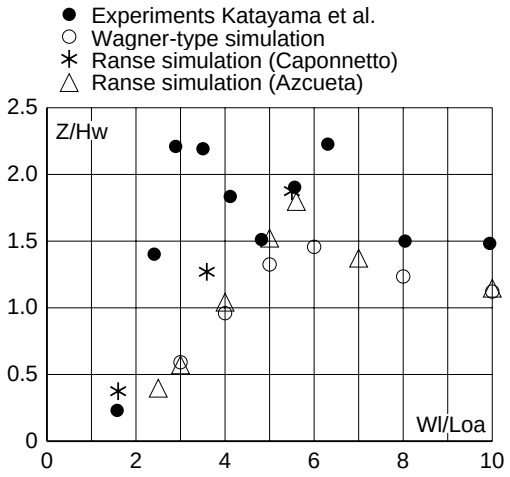

Fig. 19. Non-dimensional heave over nondimensional wave length for $H_w =$ 4cm and $U = 9$m/s

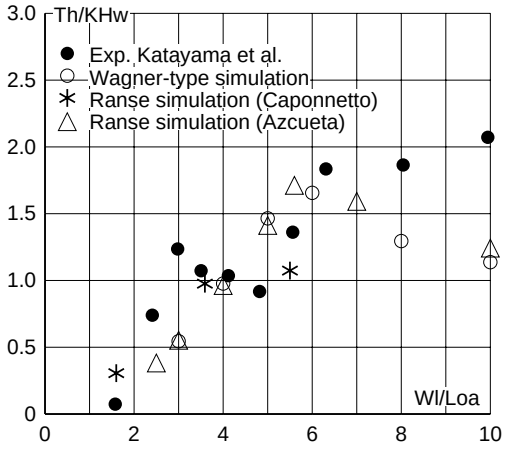

Fig. 20. Non-dimensional pitch over nondimensional wave length for $H_w =$ 4cm and $U = 9$m/s

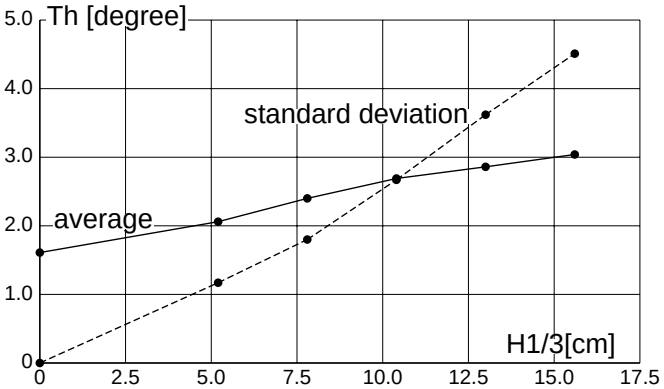

Fig. 21. Average trim and pitch standard deviation for $U = 9$m/s over significant wave height $H_{1/3}$ according to Wagner-type simulations

3. A simple, fast simulation method based on a Wagner-type approach for the forces on the boat's cross-sections results in motion predictions which are not fully satisfactory but nonetheless appear useful.

4. Simulations using the Ranse solver Comet (a finite volume method using the volume-of-fluid method to deal with the free surface) show a fair degree of robustness and reasonable coincidence with the experimental results.

5. In many cases the limit cycles appear only after a time span which appears too long both for tank experiments and for Ranse simulations.

6. Also due to the sensitivity of the responses to wave irregularities reliable measurements in regular waves are unusually difficult.

7. Different limit cycles for the same model and wave conditions but different initial conditions make both measurements and simulations, to a certain degree, a matter of random.

8. These difficulties are avoided if tests and fast-running simulations are performed in natural irregular seaways.

9 REFERENCES

AZCUETA, R., (2001), *Computation of Turbulent Free-Surface Flows Around Ships and Floating Bodies*, PhD. thesis, Technical University Hamburg-Harburg

ARMAND, J.L. and COINTE, R. (1987), *Hydrodynamic impact analysis of a cylinder*, 5th OMAE, Tokyo, Vol. I, 609-634

BERTRAM, V. (2000), *Practical Ship Hydrodynamics*, Butterworth-Heinemann editions

AZCUETA, R., (2001), *Computation of Turbulent Free-Surface Flows Around Ships and Floating Bodies*, PhD. thesis, Technical University Hamburg-Harburg

ARMAND, J.L. and COINTE, R. (1987), *Hydrodynamic impact analysis of a cylinder*, 5th OMAE, Tokyo, Vol. I, 609-634

BERTRAM, V. (2000), *Practical Ship Hydrodynamics*, Butterworth-Heinemann editions

CAMPBELL, I.M.C. and WEYNBERG, P.A. (1980), *Measurement of parameters affecting slamming*, Rep. 440, Techn. Rep. Center OT-R-8042, Southampton Univ., Wolfson Unit

CAPONNETTO, M. (2000), *Numerical Simulation of Planing Hulls*, Proceedings of 3rd NuTTS conf., Tjärnö, Sweden

CAPONNETTO, M. (2001), *Practical CFD Simulations for Planing Hulls*, HIPER '01, Hamburg

CAPONNETTO M. (2002), Sea keeping simulation of fast hard chine vessels using RANSE. 5th NuTTS, 29 September 2002, Pornichet (France)

DOBROVOLSKAYA, Z.N. (1969), *On some problems of similarity flow of fluids with a free surface*, J. Fluid Mech. 36, 805-829

v.KARMAN, T. (1929), *The impact of seaplane floats during landing*, NACA-TN 321, 8p.

KATAYAMA, T., HINAMI, T. and IKEDA, Y. (2000), *Longitudinal motion of a super high-speed planing craft in regular head waves*, Proc. 4th Osaka Colloquium on Seakeeping Performance of Ships

MEI, X.M., LIU, Y. and YUE, D.K.P. (1999), *On the water impact of general two-dimensional sections*, Aplied Ocean Res. 21, 1-15

SÖDING, H. (2001), *How to integrate free motions of solids in fluids*, NuTTS 01, Hamburg

WAGNER, H. (1932), *Über Stoß und Gleitvorgänge an der Oberfläche von Flüssigkeiten*, ZAMM 12(4), 193-215

ZHAO, R., FALTINSEN, O. and HASLUM, H. (1996), *A simplified non-linear analysis of a high-speed planing craft in calm water*, Fast'97, 431-438